Title

Picosecond ionization dynamics in femtosecond filaments at high pressures

Journal

Physical Review A, 95(1)

ISSN

2469-9926

Authors

Gao, X
Patwardhan, G
Schrauth, S
et al.

Publication Date

2017-01-25

DOI

10.1103/PhysRevA.95.013412

Peer reviewed

Picosecond ionization dynamics in femtosecond filaments at high pressures

Xiaohui Gao,[1] Gauri Patwardhan,[1,2] Samuel Schrauth,[2] Daiwei Zhu,[2] Tenio Popmintchev,[3] Henry C. Kapteyn,[3] Margaret M. Murnane,[3] Dmitri A. Romanov,[4,5] Robert J. Levis,[4,6] and Alexander L. Gaeta[1,*]

[1]*Department of Applied Physics and Applied Mathematics, Columbia University, New York, New York 10027, USA*

[2]*School of Applied and Engineering Physics, Cornell University, Ithaca, New York 14853, USA*

[3]*JILA, University of Colorado, Boulder, Colorado 80309, USA*

[4]*Center for Advanced Photonics Research, College of Science and Technology, Temple University, Philadelphia, Pennsylvania 19122, USA*

[5]*Department of Physics, Temple University, Philadelphia, Pennsylvania 19122, USA*

[6]*Department of Chemistry, Temple University, Philadelphia, Pennsylvania 19122, USA*

(Received 3 March 2016; published 25 January 2017)

We investigate the plasma dynamics inside a femtosecond-pulse-induced filament generated in an argon gas for a wide range of pressures up to 60 bar. At higher pressures, we observe ionization immediately following a pulse, with up to a threefold increase in the electron density within 30 ps after the filamentary propagation of a femtosecond pulse. Our study suggests that this picosecond evolution can be attributed to collisional ionization including Penning and associative ionizations and electron-impact ionization of excited atoms generated during the pulse. The dominance of excited atoms over ionized atoms at the end of the pulse also indicates an intrapulse inhibition of avalanche ionization. This delayed ionization dynamics provides evidence for diagnosing atomic and molecular excitation and ionization in intense laser interaction with high-pressure gases.

DOI: 10.1103/PhysRevA.95.013412

Ionization is a likely outcome of intense laser-matter interactions. Ionized electrons can be used to extract information about the laser pulse [1] or the electronic structure of molecules [2,3]. Ionization plays a critical role in other phenomena such as balancing self-focusing in femtosecond filamentation [4], achieving phase-matching in high-order harmonic generation [5], and optimizing injection in electron accelerators [6]. Various mechanisms give rise to ionization, depending on the laser conditions and target properties. Multiphoton and tunnel ionization are typically the dominant process in tenuous gases and have been extensively studied [7]. Alternatively, ionization can result from collisions of atoms with other particles, and this includes electron-impact ionization, Penning ionization (e.g., $Ar^* + Ar^* \rightarrow Ar^+ + Ar + e^-$, where Ar^* denotes an excited argon atom) and associative ionization (e.g., $Ar^* + Ar^* \rightarrow Ar_2{}^+ + e^-$). Electron-impact ionization has been shown to play an important role in laser interactions with high-pressure gases [8], clusters [9], and solids [10]. It is typically seeded by optical ionization with an ultrashort pulse, and separating and identifying these two effects is a challenging task [8,10]. Penning ionization and associative ionization, in which the ionization energy is given by the de-excitation of the excited atoms, are important processes in plasma chemistry [11] and have a characteristic time of microseconds or more in typical gas discharge. However, their role in laser-produced plasmas has been elusive and very little studied. The postpulse dynamics resulting from collisional ionization is interesting not only to provide a fundamental understanding but also to shed light on the physical processes that occur during the pulse. Measurements of postpulse electron dynamics have been made using interferometry in a hot plasma [12] or indirectly via four-wave mixing [13] or via Rabi oscillations [14]. The laser intensity used in these experiments was sufficiently high ($\geqslant 5 \times 10^{14}$ W/cm^2) so that the ponderomotive energy was comparable to the ionization potential, which gives rise to an increase in the plasma density by tens of percent in agreement with simulations [15]. However, the plasma density in weakly ionized filaments either increases by less than 1% [15] or decreases on a picosecond time scale [16] due to the low electron temperature because of the intensity clamping [17].

In this paper, we use time-resolved shadowgraphy and/or interferometry to measure the time dependence of the plasma density during and immediately following the formation of a femtosecond filament in a high-pressure argon gas. We observe a threefold increase in the electron density at the highest pressures within the first 30 ps after a plasma channel is created. Our experimental measurements, in agreement with theoretical simulations, show that the plasma density continues to rise after the pulse has passed through the interaction region due to collisional ionization of excited atoms. The presence of a significant fraction of excited atoms, which have a large nonlinearity [18] and different ionization dynamics, can potentially affect the filamentation with single and multiple pulses. In addition, these results will help to accurately interpret and control the interaction of intense laser pulses with high-pressure gases, which has given rise to many interesting phenomena such as laser-induced gas breakdown [19], generation of warm dense plasmas [20], supercontinuum generation [21], and efficient ultrahigh harmonic generation [22]. Moreover, the study of generation of excited atoms and molecules is central to the lasing action during filamentary propagation [23,24], in particular at midinfrared wavelengths, where rich electron-impact dynamics may be present since the ponderomotive energy scales as λ^2, where λ is the laser wavelength.

In our experiments, 60-fs, 800-nm pulses from a 10-Hz Ti:sapphire amplified laser system are used. The spatial profile of the beam is cleaned by a vacuum spatial filter, and the beam is split into a pump beam and a probe beam. Figure 1 shows the experimental setup in which the pump beam is focused by a lens of 20-cm focal length into a gas cell with

*a.gaeta@columbia.edu

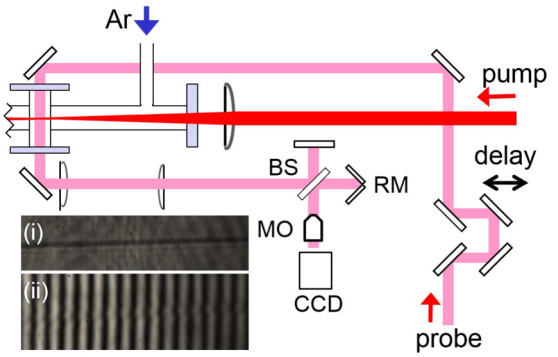

FIG. 1. Experimental setup. BS, beamsplitter; RM, rooftop mirror; MO, microscope objective. Inset (i): Shadowgraph recording plasma-induced absorption imprinted on a probe. Inset (ii): Interferogram recording plasma-induced phase alterations imprinted on a probe.

pressures ranging from 1 to 60 bar, and the energy of the pump beam is maintained at 0.3 mJ. White-light generation, which is an indication of filamentation, is observed for pressures greater than 10 bar. The unfocused probe propagates through the filament and is relay-imaged onto an externally triggered charge-coupled device using a $4f$ imaging system and a microscope objective. The spatial resolution is determined to be 12 μm, and the delay of the probe is scanned by translating a stage at each pressure. For the interferometric measurement, a Michelson scheme is used to produce the two arms, phase alterations are imprinted onto the top part of the probe, and the bottom part of the beam serves as the reference. After the spatial orientation of the beam is flipped by a rooftop mirror, the reference region is spatially overlapped with the probe region, producing an interferometric image. The shadowgraph is captured when the rooftop mirror is blocked. The shadowgraph and interferogram in Fig. 1 show the single-shot raw images captured by the charge-coupled device in the shadowgraphic and interferometric measurements, respectively.

Figure 2(a) shows two single-shot shadowgraphs at 60 bar of argon gas pressure. At $\Delta t = 0$, the shadow is so weak that a background image without a pump beam is subtracted to enhance the contrast. The ionization front allows us to determine the timing of the pump and probe. At a delay of 50 ps, the shadow is directly visible in the raw image. Figure 2(b) shows the normalized lineout at the position of dashed line in Fig. 2(a) for various delays. Figure 2(c) plots the evolution of the transmission at the axis of the plasma extracted from the shadowgraph. The transmission drops substantially during the first 30 ps and then levels off to a value slightly less than 0.6. Since the transmission is determined by the plasma absorption $e^{-\sigma N_e L}$, where σ is the absorption cross section, N_e is the electron density, and L is the effective length, the decay of transmitted light clearly indicates the rise of the electron density.

The change in electron density can also be observed directly by measuring the phase shift $\Delta\phi \propto n_e L$ of the probe beam. Figure 3(a) shows several single-shot phase images extracted from the interferogram using the Fourier transform method [25]. Considering the pulse duration of the probe and transverse dimension of the filament, the temporal resolution

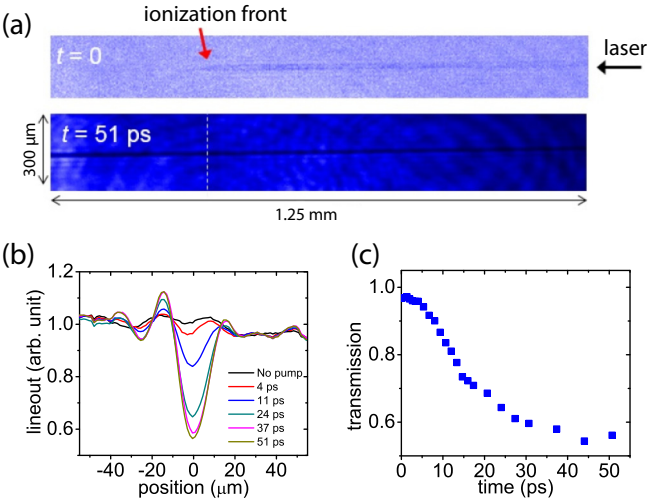

FIG. 2. (a) Single-shot shadowgraphs for two delay times. (b) Lineout measurements for several delay times (from top to bottom: 0- to 51-ps delay). Each lineout is averaged over 10 shots. Here the width of the shadow broadens due to multishot averaging. (c) Transmission extracted from the shadowgraph versus delay at 60 bar. Each data point represents a 10-shot average.

of the measurement is 100 fs. Figure 3(b) shows the phase shift at $x = 0.25$ mm in Fig. 3(a) as a function of the delay Δt for three gas pressures. While the phase shift increases by 30% at 20 bar, it increases by more than a factor of 3 within

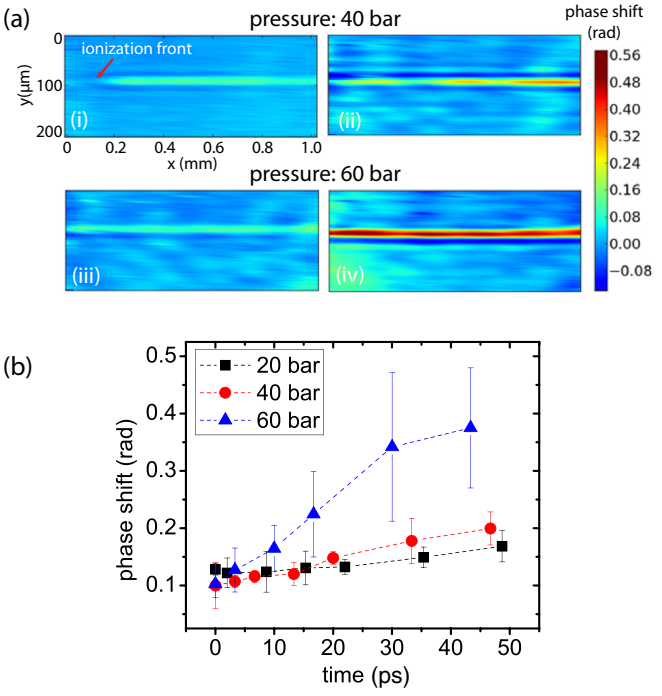

FIG. 3. (a) Single-shot phase images extracted from interferograms at $p = 40$ bar—(i) $\Delta t = 0$ and (ii) $\Delta t = 46$ ps—and at $p = 60$ bar—(iii) $\Delta t = 1$ ps and (iv) $\Delta t = 43$ ps. (b) Measured phase shifts vs delay at several pressures. Each data point is the average of 25 single-shot measurements. Error bars represent the standard deviation. The standard deviation at 60 bar is large because the position is near the end of the filament.

the first 30 ps at 60 bar. The shadowgraphic and phase-shift measurements show modulations outside the plasma filament, which is caused by the limited spatial resolution of the imaging system [26]. The oscillations at the two sides of the plasma in the shadowgraph and the phase image are not symmetric, which we believe is due to the ionization being extremely sensitive to the laser intensity near the threshold and a small asymmetry in laser intensity results in a significant asymmetry in the plasma density. The FWHM size of the filament in all the measurements is approximately 12 μm, regardless of the pressure or probe delay, which indicates that the measured size is limited by the spatial resolution of the imaging setup and the actual size may be smaller. Assuming a size of 40 μm at 1 atm for a similar focusing condition [27] and a scaling of $d \propto \sqrt{P}$ [28], where d is the diameter and P the pressure, and the predicted sizes at 20, 40, and 60 bar are approximately 8.9, 6.3, and 5.2 μm, respectively. For a 0.1-rad phase shift, the corresponding values of the degree of ionization are 0.009, 0.006, and 0.005. The absence of size variation at various delays in Fig. 2(b) indicates that the time scale of hydrodynamic expansion is much longer than that of the measurement, which is consistent with theoretical analysis since the ion sound wave needs 8 ns to travel 12 μm based on the sound speed at $T_e = 1$ eV. The laser power used in experiments is below the threshold power for a clean profile to develop multiple filamentation [29], thus a single filament is formed. Multifilamentation is observed when the input profile is polluted by a damage spot on the mirror or when a vortex beam is used. Filamentation in a high-pressure nitrogen gas is also investigated, but the phase shift is below the noise level. We believe that the different dynamics is due to the electron-impact dissociation of N_2 by the quivering electrons.

To understand the mechanism for the observed picosecond ionization after the pulse, numerical simulations are performed. We assume that variables have no spatial dependence since hydrodynamics expansion can be neglected. The postpulse time evolution of the atom density and electron temperature T_e follows a system of rate equations where the particle balance is described by

$$\frac{dN_j}{dt} = -\sum_k a_{jk} W_{j\to k} N_j + \sum_l W_{l\to j} N_l, \qquad (1)$$

where N_j is the density of species j, a_{jk} is the stoichiometric coefficient of the atoms, and W is the rate of reactions including electron-impact excitation and ionization, Penning ionization, associative ionization, three-body recombination, and dissociative recombination. The electron temperature T_e obeys the equation [30,31]

$$\frac{d}{dt}\left(\frac{3}{2} N_e T_e\right) = -\sum_j \sum_k \varepsilon_{jk} W_{j\to k} N_j, \qquad (2)$$

where ε_{jk} is the energy loss or gain of the electrons in various reactions. The included reactions and the rate coefficients are listed in the Appendix. The reaction rate scales with the density of the reactant, and the initial values also show pressure dependence.

We simulate the evolution in 60 bar of argon gas starting at $t_0 = 200$ fs, at which time the electrons have thermalized. We use the initial normalized electron density $N_{e,0} = 0.005$ taken from the measurement. The results are sensitive to the initial densities of atoms in $4s$ and $4p$ states $N_{4s,0}$ and $N_{4p,0}$. The initial temperature $T_{e,0}$ and the densities of other species primarily affect the dynamics within the first picosecond, for which we do not observe much change in the experiment. Thus we assume that $T_{e,0} = 2$ eV and densities of other species are 0. Figure 4(a) shows the result for $N_{4s,0} = 0.025$ and $N_{4p,0} = 0.02$, in which the rise time and amplitude approximately match the measured values. Here, the numbers of excited atoms are not depleted since electron-ion recombination generates excited atoms as well. Thus, ionization and recombination reach a dynamic equilibrium which lasts until the diffusion or radiative recombination can no longer be neglected. If $N_{\text{excited},0} \ll N_{e,0}$ and T_e is high, rapid ionization occurs within the first picosecond due to the high atom density, causing T_e to decrease to approximately 2 eV. Further ionization can only occur from a tiny fraction of electrons in the high-energy tail of the thermal distribution. When $N_{\text{excited},0} \gg N_{e,0}$, electron-impact ionization of excited atoms alone cannot reproduce the observed picosecond multifold increase, as shown in the dash-dotted green curve in Fig. 4(b). Penning and associative ionization plays a central role not only for the direct generation of electrons but also for the release of energy

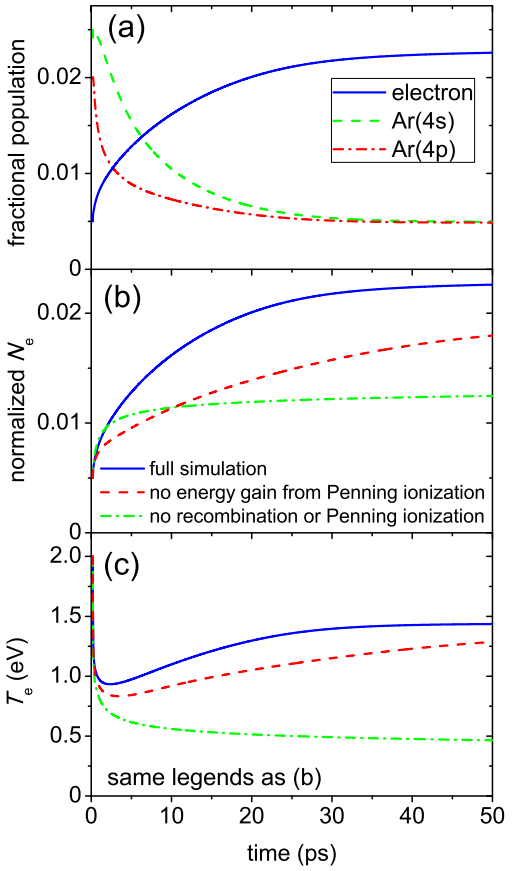

FIG. 4. (a) Time evolution of the normalized density of electrons and excited atoms. (b) Time evolution of the normalized electron density N_e with (solid blue line) and without (dashed red line) the energy gain from Penning ionization and when recombination and Penning ionization are not included (dash-dotted green line). (c) Time evolution of T_e for the same condition as in (b).

to the electrons, which prevents T_e from decreasing and further assists ionization through electron-impact. The effect of the heating of Penning ionization can be seen from the solid blue curve and dashed red curve in Figs. 4(b) and 4(c). Here the evolutions of N_e and T_e with (solid blue curve) and without (dashed red curve) energy gain from the Penning ionization are presented. These simulations confirm that most of the ionization after the pulse is due to excited atoms in which the concentration is nearly one order of magnitude higher than that of ionized atoms.

Excited atoms can be generated by electron-impact excitation, frustrated tunnel ionization [32], or electron-ion recombination. Frustrated tunnel ionization is almost absent for pulses with circular polarization [32]. However, we observe similar picosecond ionization using circularly polarized pulses. Three-body recombination into excited states is included in the postpulse simulation, but the corresponding characteristic time is much longer than the pulse duration, so its contribution to initial excited atoms is not significant. We thus conclude that electron-impact excitation is the dominant mechanism responsible for excited atoms immediately after the pulse. For ultrashort-pulse filamentation electron-impact ionization is typically modeled under the assumption that all the absorbed energy is dedicated to ionizing the gas. However, the excitation has a lower threshold than ionization, so when the released electrons gain energy through inverse Bremsstrahlung, this energy is mostly channeled to the electron-impact excitation when the collision frequency is high, thus effectively depleting the number of electrons with an energy above the ionization energy and substantially inhibiting electron-impact ionization.

In summary, we have investigated the temporal evolution of plasma filaments produced by near-infrared femtosecond laser pulses in a high-pressure argon gas using picosecond-time-resolved transverse interferometry and shadowgraphy. The plasma density increases several times in the wake of femtosecond laser pulses, and this represents, to our knowledge, the first observation of collisional ionization of excited atoms in a laser-induced filament. Our experimental observation is confirmed by simulations and reveals that intrapulse avalanche ionization is diverted to electronic excitation. This indicates that avalanche ionization during the laser pulse can possibly be inhibited, in contrast to the enhanced ionization in laser-cluster interaction. The dependence of collisional excitation and ionization on various parameters, such as pulse duration and wavelength, is worth further investigation. We believe this effect exists at lower pressure for longer pulse durations. Ultimately, these results are important for characterization of impact ionization and excitation in the presence of a laser field [33] and for experiments that involve multiple time-delayed pulses for filament and ionization control [34–36], in particular, at high pressures or at midinfrared wavelengths.

This work was supported by the AFSOR Multidisciplinary University Research Initiative under Grant No. FA9550-10-1-0561 and the DARPA PULSE program.

APPENDIX

In this appendix we list reaction processes and rate coefficients used in our model.

Reaction process	Rate coefficient (cm^3/s)	Ref. No.(s.)
Electron-impact excitation		
$e + \mathrm{Ar} \rightarrow e + \mathrm{Ar}(4s)$	$1.45 \times 10^{-8} e^{-12.96/T_e}$	[37]
$e + \mathrm{Ar} \rightarrow e + \mathrm{Ar}(4p)$	$2.12 \times 10^{-8} e^{-13.13/T_e}$	[37]
$e + \mathrm{Ar} \rightarrow e + \mathrm{Ar}(3d,5s)$	$1.22 \times 10^{-8} e^{-17.8/T_e}$	[37]
$e + \mathrm{Ar} \rightarrow e + \mathrm{Ar}(4d)$	$8 \times 10^{-9} e^{-19.05/T_e}$	[37]
$e + \mathrm{Ar} \rightarrow e + Ar(\mathrm{hl})$	$8.29 \times 10^{-9} e^{-18.14/T_e}$	[37]
$e + \mathrm{Ar}(4s) \rightarrow e + \mathrm{Ar}(4p)$	$8.9 \times 10^{-7} T_e^{0.51} e^{-1.59/T_e}$	[38]
$e + \mathrm{Ar}(4p) \rightarrow e + \mathrm{Ar}(4s)$	$3 \times 10^{-7} T_e^{0.51}$	[39]
Electron-impact ionization		
$e + \mathrm{Ar} \rightarrow e + e + \mathrm{Ar}^+$	$S(T_e)$	[40]
$e + \mathrm{Ar}(4s) \rightarrow e + e + \mathrm{Ar}^+$	$2 \times 10^{-7} e^{-6.2/T_e}$	[41,42]
$e + \mathrm{Ar}(4p) \rightarrow e + e + \mathrm{Ar}^+$	$2 \times 10^{-6} e^{-4.4/T_e}$	[41,42]
$e + \mathrm{Ar}(3d,5s) \rightarrow e + e + \mathrm{Ar}^+$	$6 \times 10^{-6} e^{-2.4/T_e}$	[41,42]
$e + \mathrm{Ar}(4d) \rightarrow e + e + \mathrm{Ar}^+$	$2 \times 10^{-5} e^{-2.2/T_e}$	[41,42]
$e + \mathrm{Ar}(\mathrm{hl}) \rightarrow e + e + \mathrm{Ar}^+$	$2 \times 10^{-4} e^{-0.5/T_e}$	[41,42]
Penning ionization		
$\mathrm{Ar}(4s) + \mathrm{Ar}(4s) \rightarrow \mathrm{Ar}^+ + e + \mathrm{Ar}$	5×10^{-10}	[42,43]
$\mathrm{Ar}(4s) + \mathrm{Ar}(4p) \rightarrow \mathrm{Ar}^+ + e + \mathrm{Ar}$	5×10^{-10}	[42,43]
$\mathrm{Ar}(4s) + \mathrm{Ar}(3d,5s) \rightarrow \mathrm{Ar}^+ + e + \mathrm{Ar}$	5×10^{-10}	[42,43]
$\mathrm{Ar}(4s) + \mathrm{Ar}(4d) \rightarrow \mathrm{Ar}^+ + e + \mathrm{Ar}$	5×10^{-10}	[42,43]
$\mathrm{Ar}(4s) + \mathrm{Ar}(\mathrm{hl}) \rightarrow \mathrm{Ar}^+ + e + \mathrm{Ar}$	5×10^{-10}	[42,43]
Associative ionization		
$\mathrm{Ar}(4s) + \mathrm{Ar}(4s) \rightarrow e + \mathrm{Ar}_2^+$	5×10^{-10}	[42]
Three-body recombination		
$e + e + \mathrm{Ar}^+ \rightarrow e + \mathrm{Ar}$	Calculated by	[44]
$e + e + \mathrm{Ar}^+ \rightarrow e + \mathrm{Ar}(4s)$	detailed balance	
$e + e + \mathrm{Ar}^+ \rightarrow e + \mathrm{Ar}(4p)$	from the reverse	
$e + e + \mathrm{Ar}^+ \rightarrow e + \mathrm{Ar}(3d,5s)$	process,	
$e + e + \mathrm{Ar}^+ \rightarrow e + \mathrm{Ar}(4d)$	electron-impact	
$e + e + \mathrm{Ar}^+ \rightarrow e + \mathrm{Ar}(\mathrm{hl})$	ionization	
Dissociative recombination		
$e + \mathrm{Ar}_2^+ \rightarrow \mathrm{Ar} + \mathrm{Ar}(4p)$	$9 \times 10^{-7} T_e^{-0.67}$	[45]

[1] M. G. Pullen, W. C. Wallace, D. E. Laban, A. J. Palmer, G. F. Hanne, A. N. Grum-Grzhimailo, K. Bartschat, I. Ivanov, A. Kheifets, D. Wells, H. M. Quiney, X. M. Tong, I. V. Litvinyuk, R. T. Sang, and D. Kielpinski, Phys. Rev. A **87**, 053411 (2013).

[2] M. Meckel, D. Comtois, D. Zeidler, A. Staudte, D. Pavičić, H. C. Bandulet, H. Pépin, J. C. Kieffer, R. Dörner, D. M. Villeneuve, and P. B. Corkum, Science **320**, 1478 (2008).

[3] H. Conrad, G. Ertl, J. Küppers, S. W. Wang, K. Gérard, and H. Haberland, Phys. Rev. Lett. **42**, 1082 (1979).

[4] A. Braun, G. Korn, X. Liu, D. Du, J. Squier, and G. Mourou, Opt. Lett. **20**, 73 (1995).

[5] T. Popmintchev, M.-C. Chen, A. Bahabad, M. Gerrity, P. Sidorenko, O. Cohen, I. P. Christov, M. M. Murnane, and H. C. Kapteyn, Proc. Natl. Acad. Sci. USA **106**, 10516 (2009).

[6] C. McGuffey, A. G. R. Thomas, W. Schumaker, T. Matsuoka, V. Chvykov, F. J. Dollar, G. Kalintchenko, V. Yanovsky, A. Maksimchuk, K. Krushelnick, V. Y. Bychenkov, I. V. Glazyrin, and A. V. Karpeev, Phys. Rev. Lett. **104**, 025004 (2010).

[7] P. Agostini and L. F. DiMauro, Adv. At. Mol. Opt. Phys. **61**, 117 (2012).

[8] W. M. Wood, C. W. Siders, and M. C. Downer, Phys. Rev. Lett. **67**, 3523 (1991).

[9] B. Schütte, M. Arbeiter, A. Mermillod-Blondin, M. J. J. Vrakking, A. Rouzée, and T. Fennel, Phys. Rev. Lett. **116**, 033001 (2016).

[10] D. Grojo, M. Gertsvolf, S. Lei, T. Barillot, D. M. Rayner, and P. B. Corkum, Phys. Rev. B **81**, 212301 (2010).

[11] P. E. Siska, Rev. Mod. Phys. **65**, 337 (1993).

[12] S. V. Garnov, V. V. Bukin, A. A. Malyutin, and V. V. Strelkov, AIP Conf. Proc. **1153**, 37 (2009).

[13] A. Filin, R. Compton, D. A. Romanov, and R. J. Levis, Phys. Rev. Lett. **102**, 155004 (2009).

[14] R. Compton, A. Filin, D. A. Romanov, and R. J. Levis, Phys. Rev. Lett. **103**, 205001 (2009).

[15] D. A. Romanov and R. J. Levis, Phys. Rev. A **87**, 063410 (2013).

[16] J. K. Wahlstrand, Y. H. Chen, Y. H. Cheng, S. R. Varma, and H. M. Milchberg, IEEE J. Quantum Electron. **48**, 760 (2012).

[17] A. Becker, N. Aközbek, K. Vijayalakshmi, E. Oral, C. Bowden, and S. Chin, Appl. Phys. B **73**, 287 (2001).

[18] P. M. Paul, T. O. Clatterbuck, C. Lyngå, P. Colosimo, L. F. DiMauro, P. Agostini, and K. C. Kulander, Phys. Rev. Lett. **94**, 113906 (2005).

[19] R. G. Meyerand and A. F. Haught, Phys. Rev. Lett. **11**, 401 (1963).

[20] A. Bataller, G. R. Plateau, B. Kappus, and S. Putterman, Phys. Rev. Lett. **113**, 075001 (2014).

[21] P. B. Corkum, C. Rolland, and T. Srinivasan-Rao, Phys. Rev. Lett. **57**, 2268 (1986).

[22] T. Popmintchev, M.-C. Chen, D. Popmintchev, P. Arpin, S. Brown, S. Ališauskas, G. Andriukaitis, T. Balčiunas, O. D. Mücke, A. Pugzlys, A. Baltuška, B. Shim, S. E. Schrauth, A. Gaeta, C. Hernández-García, L. Plaja, A. Becker, A. Jaron-Becker, M. M. Murnane, and H. C. Kapteyn, Science **336**, 1287 (2012).

[23] D. Kartashov, S. Ališauskas, G. Andriukaitis, A. Pugžlys, M. Shneider, A. Zheltikov, S. L. Chin, and A. Baltuška, Phys. Rev. A **86**, 033831 (2012).

[24] S. Mitryukovskiy, Y. Liu, P. Ding, A. Houard, A. Couairon, and A. Mysyrowicz, Phys. Rev. Lett. **114**, 063003 (2015).

[25] M. Takeda, H. Ina, and S. Kobayashi, J. Opt. Soc. Am. **72**, 156 (1982).

[26] P. Blanc, P. Audebert, F. Falliès, J. P. Geindre, J. C. Gauthier, A. D. Santos, A. Mysyrowicz, and A. Antonetti, J. Opt. Soc. Am. B **13**, 118 (1996). B. T. Bowes, H. Langhoff, M. C. Downer, M. Wilcox, B. Hou, J. Nees, and G. Mourou, Opt. Lett. **31**, 116 (2006).

[27] F. Théberge, W. Liu, P. T. Simard, A. Becker, and S. L. Chin, Phys. Rev. E **74**, 036406 (2006).

[28] S. Hosseini, O. Kosareva, N. Panov, V. P. Kandidov, A. Azarm, J.-F. Daigle, A. B. Savel'ev, T.-J. Wang, and S. L. Chin, Laser Phys. Lett. **9**, 868 (2012).

[29] G. Fibich, S. Eisenmann, B. Ilan, Y. Erlich, M. Fraenkel, Z. Henis, A. L. Gaeta, and A. Zigler, Opt. Express **13**, 5897 (2005).

[30] X. Gao, A. V. Arefiev, R. C. Korzekwa, X. Wang, B. Shim, and M. C. Downer, J. Appl. Phys. **114**, 034903 (2013).

[31] D. A. Romanov, R. Compton, A. Filin, and R. J. Levis, Phys. Rev. A **81**, 033403 (2010).

[32] T. Nubbemeyer, K. Gorling, A. Saenz, U. Eichmann, and W. Sandner, Phys. Rev. Lett. **101**, 233001 (2008).

[33] P. P. Rajeev, M. Gertsvolf, P. B. Corkum, and D. M. Rayner, Phys. Rev. Lett. **102**, 083001 (2009).

[34] Z. Henis, G. Milikh, K. Papadopoulos, and A. Zigler, J. Appl. Phys. **103**, 103111 (2008); P. Polynkin and J. V. Moloney, Appl. Phys. Lett. **99**, 151103 (2011).

[35] Y. Liu, A. Houard, B. Prade, S. Akturk, A. Mysyrowicz, and V. T. Tikhonchuk, Phys. Rev. Lett. **99**, 135002 (2007).

[36] L. Shi, W. Li, Y. Wang, X. Lu, L. Ding, and H. Zeng, Phys. Rev. Lett. **107**, 095004 (2011).

[37] E. Eggarter, J. Chem. Phys. **62**, 833 (1975).

[38] F. Kannari, M. Obara, and T. Fujioka, J. Appl. Phys. **57**, 4309 (1985).

[39] S. Ashida, C. Lee, and M. A. Lieberman, J. Vac. Sci. Technol. A **13**, 2498 (1995).

[40] W. Lotz, Z. Phys. A **216**, 241 (1968).

[41] H. Deutsch, K. Becker, A. N. Grum-Grzhimailo, K. Bartschat, H. Summers, M. Probst, S. Matt-Leubner, and T. D. Märk, Int. J. Mass Spectrom. **233**, 39 (2004).

[42] X. M. Zhu and Y. K. Pu, J. Phys. D: Appl. Phys. **43**, 015204 (2010).

[43] N. B. Kolokolov and A. B. Blagoev, Phys. Usp. **36**, 152 (1993).

[44] N. H. Burnett and G. D. Enright, IEEE J. Quantum Electron. **26**, 1797 (1990).

[45] Y.-J. Shiu and M. A. Biondi, Phys. Rev. A **17**, 868 (1978).